Original Article

Large adipose tissue generation in a mussel-inspired bioreactor of elastic–mimetic cryogel and platelets

Journal of Tissue Engineering
Volume 9: 1–16

DOI: 10.1177/2041731418808633
journals.sagepub.com/home/tej
SAGE

Qiang Chang[1,2], Junrong Cai[1], Ying Wang[3], Ruijia Yang[2], Malcolm Xing[1,2,3] and Feng Lu[1]

Abstract

Soft tissue generation, especially in large tissue, is a major challenge in reconstructive surgery to treat congenital deformities, posttraumatic repair, and cancer rehabilitation. The concern is along with the donor site morbidity, donor tissue shortage, and flap necrosis. Here, we report a dissection-free adipose tissue chamber–based novel guided adipose tissue regeneration strategy in a bioreactor of elastic gelatin cryogel and polydopamine-assisted platelet immobilization intended to improve angiogenesis and generate large adipose tissue in situ. In order to have matched tissue mechanics, we used 5% gelatin cryogel as growth substrate of bioreactor. Platelets from the platelet-rich plasma were then immobilized onto the gelatin cryogel with the aid of polydopamine to form a biomimetic bioreactor (polydopamine/gelatin cryogel/platelet). Platelets on the substrate led to a sustained high release in both platelet-derived growth factor and vascular endothelial growth factor compared with non-polydopamine-assisted group. The formed bioreactor was then transferred to a tissue engineering chamber and then inserted above inguinal fat pad of rats without flap dissection. This integrate strategy significantly boomed the vessel density, stimulated cellular proliferation, and upregulated macrophage infiltration. There was a noticeable rise in the expression of dual-angiogenic growth factors (platelet-derived growth factor and vascular endothelial growth factor) in chamber fluid; host cell migration and host fibrous protein secretion coordinated with gelatin cryogel degradation. The regenerated adipose tissue volume gained threefold larger than control group ($p < 0.05$) with less fibrosis tissue. These results indicate that a big well-vascularized three-dimensional mature adipose tissue can be regenerated using elastic gel, polydopamine, platelets, and small fat tissue.

Keywords

Biomimetic reactor, large adipose tissue generation, elastic cryogel, tissue engineering chamber

Date received: 15 July 2018; accepted: 26 September 2018

Introduction

Adipose tissue regeneration and implantation have been considered as a promising strategy to repair soft tissue defect.[1–3] Tissue engineering chamber (TEC) induces the recipient bed to regenerate fully vascularized tissue by inserting an island fat flap with arteriovenous pedicle in a polycarbonate chamber.[4–6] Unlike scaffold-cell paradigm in tissue engineering, TEC exploits the underlying tissue's regenerative capacity rather than ex vivo tissue manipulation, and a large volume of mature soft tissue can be generated with this technique in a porcine model; however, some issues, for example, key vascular pedicle spasm and torsion or obstruction due to vessel dissection, impair its reliability and lead to devastating regeneration failure.[7,8]

[1]Department of Plastic Surgery, Nanfang Hospital, Southern Medical University, Guangzhou, China
[2]Department of Mechanical Engineering, University of Manitoba, Winnipeg, MB, Canada
[3]State Key Laboratory of Trauma, Burn and Combined Injury, Institute of Burn Research, Southwest Hospital, Third Military Medical University, Chongqing, China

Corresponding authors:
Malcolm Xing, Department of Mechanical Engineering, Nanfang Hospital, University of Manitoba, Winnipeg, MB R3T 2N2, Canada.
Email: malcolm.xing@umanitoba.ca

Feng Lu, Department of Plastic Surgery, Nanfang Hospital, Southern Medical University, Guangzhou 510515, China.
Email: doctorlufeng@hotmail.com

Large soft tissue reconstruction is a major challenge in plastic and reconstructive surgery.[9] We reported a universal dissection-free approach using a dome-like chamber to cover the fat pad, and the chamber successfully stimulated tissue to grow without involving dissection of arteriovenous pedicle.[10] The dissection-free concept eliminates the primary concern about construction failure by primary vessel pedicle spasm or obstruction. However, it is unable to induce large volume of adipose tissue. It is because the vessel-dissection-free concept does not lead to a severe trauma and thus initiating no sufficient host response at the very beginning to crease ample provisional matrix deposition for affluent angiogenesis. A pertinent improvement is needed to overcome the bottleneck in large adipose tissue regeneration.

Here, we report an integration of a matched mechanical elastic gel and active-agent "machine," platelets (Plts), enhanced immobilization via mussel-inspired catechol. Substrate's stiffness can regulate the adipose-derived stem cells' (ADSCs) adipogenesis.[10,11] Gelatin is a denatured collagen and has been used widely owing to biocompatibility, degradability, and low immunogenic.[12] Functioned the amine group of gelatin side chain with methacrylate group was used extensively to make it to stable hydrogels after copolymerization. Most recently, gelatin cryogel (GC) based on methacrylated gelatin (gelatin-MA) produced microporous structures by forming ice crystals at subzero leading to remarkably compressive elasticity.[13] The elasticity and modulus of gelatin are tunable by changing concentration and temperature.[14] In this way, stiffness mimetic of adipose tissue using GC scaffold can be produced.

Sufficient vascularization throughout the regeneration is another essential requirement for successful tissue construction. Autologous platelet-rich plasma (PRP) containing numerous angiogenesis growth factors has been used to promote tissue vascularization and regeneration.[15–18] However, PRP does not remain locally after direct injection, more than 90% growth factors released from α-granule after activation will diffuse out in tissue fluid quickly. An efficient immobilization system for Plts is required to stabilize the supplemented Plts and growth factors in targeted area in vivo. Polydopamine (pDA) can deposit on variety of substrates[19,20] in alkaline conditions through catechol functional groups followed by oxidative conversion of catechol to quinine.[21,22] Various nucleophiles, including amine, thiol, and imidazole, can be linked to catechol groups in a pDA layer.[23,24] Thus, we hypothesize that pDA can immobilize Plts to cryogel and then to improve localized growth factor release.

Realizing the primary roles of provisional self-synthesized matrix deposition, neovascularization in large tissue regeneration,[25] and stiffness match of host–guest tissue, we conceived a bioreactor to integrate TEC with angiogenic growth factors to guide adipose tissue regeneration. Highly flexible and stiffness-matched GC mimicking the stiffness of adipose tissue can be used as alternative provisional matrix substitute to support adipose progenitor cell migration, proliferation, and differentiation in niche; pDA-aided immobilization of Plt-facilitated macrophage and adipose progenitor cells chemotaxis to promote angiogenesis and adipogenesis. Thus, a large volume of adipose tissue can be made (Figure 1).

Materials and methods

Preparation of gelatin-MA and GC and mechanical properties measurement

Gelatin-MA was synthesized as described in the previous literature.[26,27] Type A gelatin (Ward's Science, Henrietta, NY, USA) was dissolved in phosphate buffered saline (PBS; Thermo Fisher Scientific, Burlington, ON, Canada) to 10 wt% at 40°C for 1 h. Methacrylic anhydride (MA; Sigma-Aldrich Co. LLC, Oakville, ON, Canada) was added dropwise to a final volume ratio of 1:4 (MA:gelatin solution). The compound was stirred at 40°C for 1 h and then diluted with 5× PBS. The mixture was dialyzed in dialysis tubing with a 10-kDa molecular weight cut-off (Thermo Fisher Scientific, Burlington, ON, Canada.). The resulting solution was lyophilized and stored at −20°C for further use.

Gelatin-MA was dissolved in deionized water (DW) (2 and 5 wt%), ammonium persulfate (APS; 0.5% w/v, Sigma-Aldrich Co. LLC, Oakville, ON, Canada), and tetramethylethylenediamine (TEMED; 0.1% w/v, Sigma-Aldrich Co. LLC, Oakville, ON, Canada) were added to the solution. The pre-solution was transferred to a cylindrical mold (8 mm in diameter, 10-mm high) and placed at −20°C to allow cryopolymerization process for 20 h.[28]

Then, we applied the mechanical tests on GC and gelatin-MA hydrogel synthesized at room temperature (cylinder, 10-mm high and 8 mm in diameter), after equilibrium swelling in PBS, compression tests were performed by Instron 5965 (Instron; Norwood, MA, USA) with a 500-N load cell at rate of 2 mm/min. Conventional gelatin hydrogel synthesized at room temperature (RT-GelMA) was set as control group. The rheological properties of RT-GelMA and GC were tested by rheometer (TA Discovery HR-1 Rheometers; TA Instruments, New Castle, DE, USA) with a 8-mm parallel plate configuration. The amplitude oscillation was conducted at 10 rad/s of angular frequency, and the sweep strain was raised from 0.1% to 100%.

pDA coating

GC was coated with a pDA layer following the previously reported method. The GC scaffolds were immersed in a dopamine (DA) solution (2 mg/mL in 10-mM Tris-HCl, pH 8.5, Sigma, St. Louis, MO, USA) and placed on a

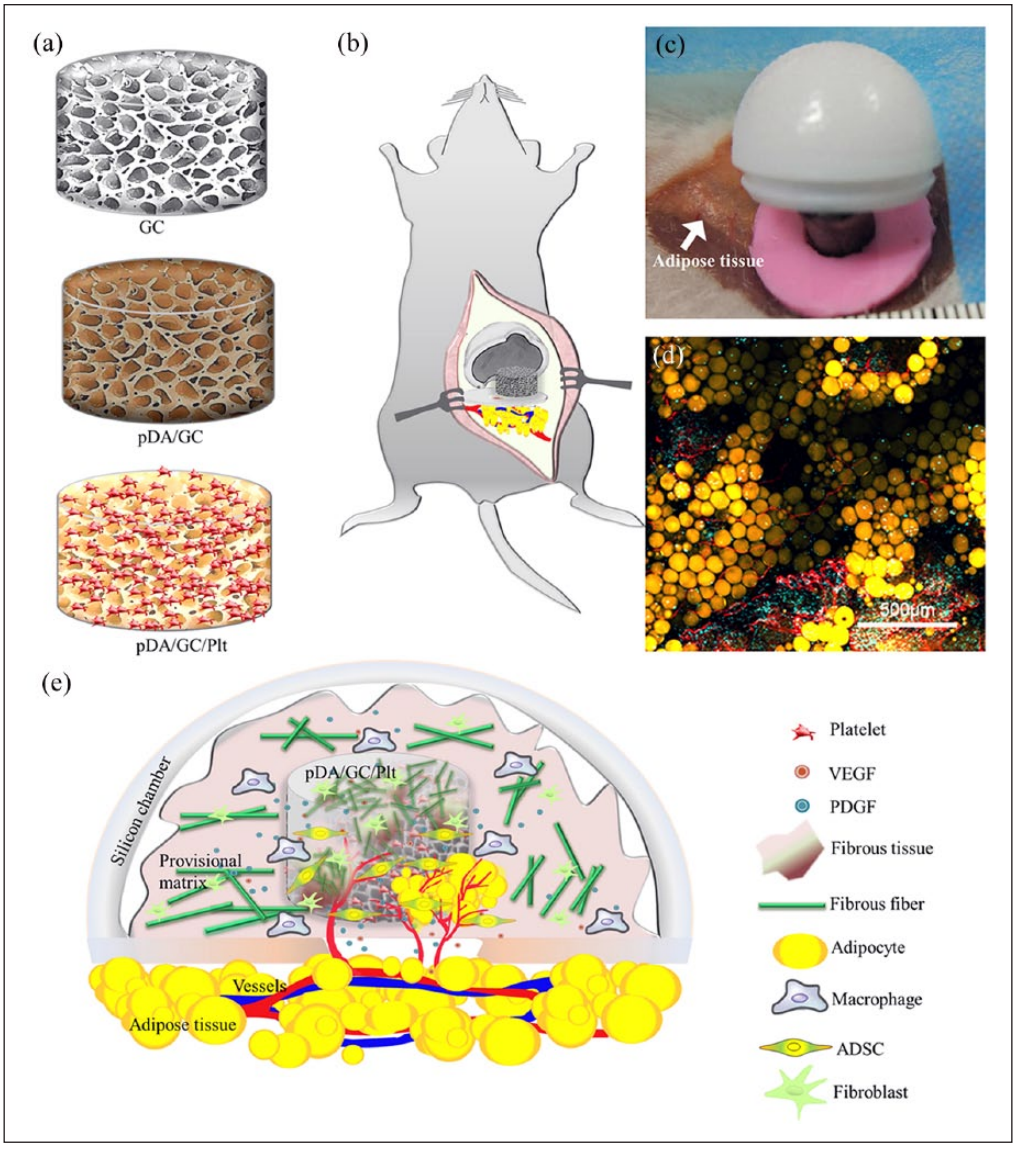

Figure 1. Schematic illustration of procedure of pDA (polydopamine)-assisted immobilization of Plt (platelet) on GC (gelatin cryogel) scaffold for guiding de novo adipose tissue regeneration: (a) immobilizing process of pDA and Plt on GC; (b) composite of pDA/GC/Plt and the chamber were anchored on the fat pad directly without traditional flap-dissection approach; (c) intraoperative view upon the dissection-free procedure; (d) regenerated adipose tissue exhibited typical lobular fat tissue structure including extensive vascularization and mature adipocytes; (e) GC acted as a bioreactor for adipose progenitor cell migration, proliferation, differentiation, and regeneration of adipose tissue.

shaker for 6 h at room temperature. The pDA-coated scaffolds were then rinsed with PBS to remove unattached DA molecules (Figure 2(a)).

Fourier transform infrared spectroscopy analysis

The infrared reflection absorption spectra of pristine gelatin, gelatin-MA, and pDA/GC were characterized using an iTR-ATR spectrometer (Nicolet iS10; Thermo Fisher Scientific Inc., Waltham, MA, USA). The absorbance spectra were collected at 32 scans with a spectral frequency ranging from 4000–500 cm^{-1}.

PRP preparation and immobilization of Plts

PRP was prepared following a reported meth. Briefly, rat blood (5 mL) was obtained from caudal vein and centrifuged at a low speed (450*g*) for 10 min. The supernatant plasma with the buffy coat was collected and further centrifuged at 850*g* for 10 min. The bottom layer was collected as PRP. The pDA/GC or GC scaffolds were immersed in 1 mL of PRP solution and placed on a shaker for 6 h at room temperature. The scaffolds were then rinsed with PBS to remove unattached Plts. The immobilized Plt number, defined as the difference between the plate count

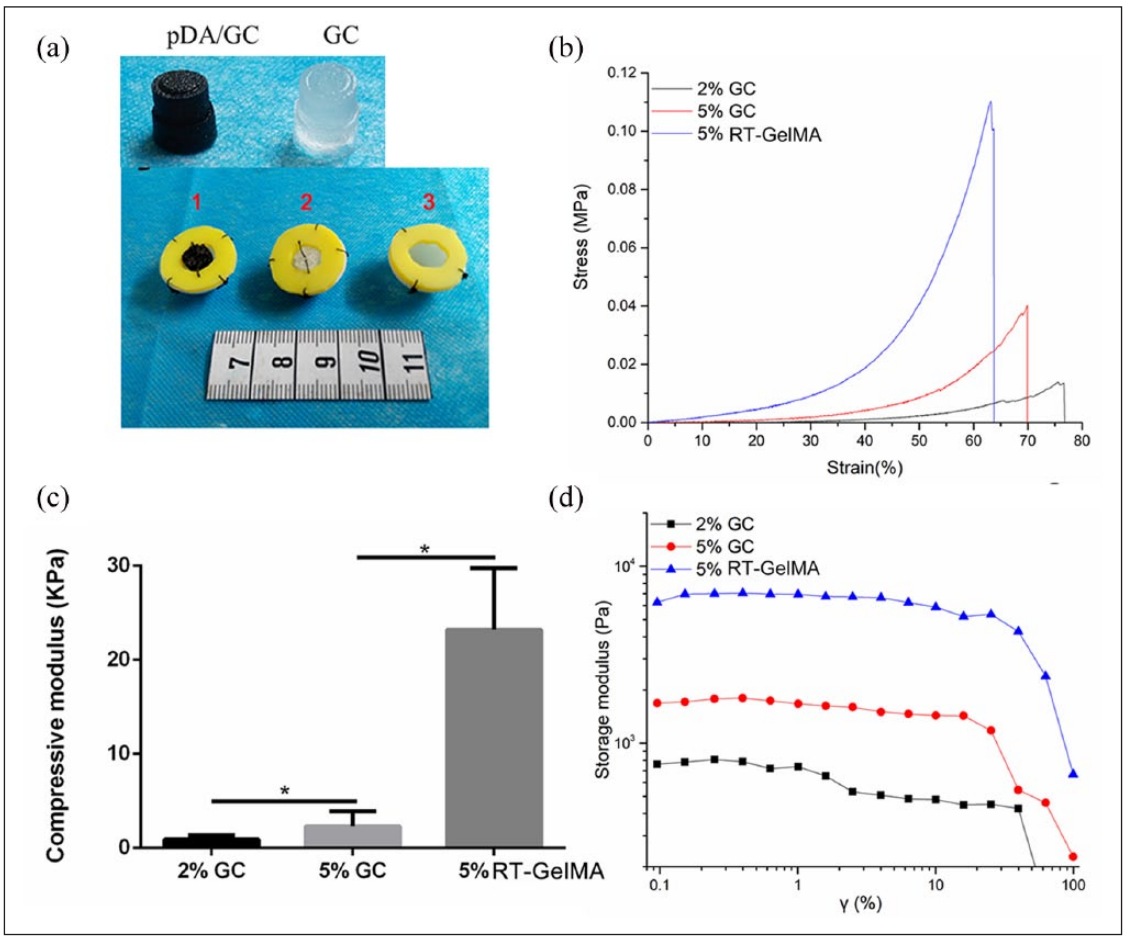

Figure 2. Mechanical properties of gelatin-MA hydrogel (RT-GelMA) and GC. (a) Transparent GC (right) and a dark brown pDA/GC scaffold (left) was fabricated for following Plt immobilization (above); tissue regeneration model with different content pDA/GC/Plt (1), GC (2), and without scaffold (3) (below). (b) Uniaxial compression strain-stress curves of 2% and 5% GC and 5% RT-GelMA. (c) Compressive modulus and (d) oscillatory strain behavior of GC and RT-GelMA (*$p < 0.05$).

in the PRP solution before and after the scaffolds were immersed ($C_{immobilization} = C_{before} - C_{after}$), was calculated for both scaffolds. The Plt concentration in the scaffold was calculated by dividing the scaffold-immobilized Plt count by the scaffold volume (0.5 mL). An automated hematology analyzer (XS-800i, Sysmex, Kobe, Japan) was used for Plt count.

Morphology of the GC scaffold with immobilized Plts

The inner sections and bottom layer of GC, RT-GelMA, pDA/GC, and pDA/GC/Plt were coated with platinum sputter and observed in a scanning electron microscope (Hitachi Company, Tokyo, Japan) at an acceleration voltage of 10 kV. The pore size of each specimen was analyzed from SEM images by ImageJ software. The interconnected porosity of the cryogel and RT-GelMA samples was further analyzed by water replacement method with slight modifications.[29,30] The samples were immersed in water for 24 h, and the fully swelled samples were weighted, followed by dehydrating with Kimwipe to totally blot off water in interconnected pores; the percentage of interconnected porosity was calculated as the ratio of sample weight change with fully swollen and dehydrated ones.

Cytotoxicity and cell proliferation measurements

The cytotoxicity of Adipose-derived Stem Cell (ASCs) was determined using a Dojindo Cell Count Kit-8 (CCK-8; Kumamoto Techno Research Park, Tokyo, Japan). Briefly, cells were seeded in 96-well plates at 3×10^3 cells/well. After adhesion, cells were incubated for 1, 3, 6, 12, 24, and 48 h with GC, pDA/GC, and pDA/GC/Plt. The solution was then replaced with 100 μL of Dulbecco's Modified Eagle Medium (DMEM), and 10 μL of the CCK-8 reagent was added. The solution was incubated for 2 h. Finally, the relative growth rate (RGR) was determined from the absorbance at 450 nm measured with a

microplate reader (Bio-Rad, Hercules, CA, USA) according to the following formula: RGR (%) = OD (test)/OD (control) ×100%. Cells that were not seeded on the material were used as the control.

In vitro growth factor release study

Upon immobilization of the Plts onto pDA/GC, the scaffold was immersed in 2 mL of PBS. In the control group, 1 mL of PBS was added to PRP to achieve a final volume of 2 mL. The release of platelet-derived growth factor (PDGF) and vascular endothelial growth factor (VEGF) from pDA/GC/Plt and PRP solution was evaluated at 1, 3, 5, 12, 24, 48, and 72 h; 5 μL of supernatant from pDA/GC/Plt and PRP solution was centrifuged for 5 min at 450*g*. This mixture was analyzed with enzyme-linked immunosorbent assay (ELISA) using PDGF and VEGF ELISA kits (R&D Systems, Minneapolis, MN, USA) following the manufacturer's instructions.

In vivo studies

After pDA coating, the GC color changes from transparent to brown (Figure 2(a)). Before Plts immobilization, the pDA/GC was sterilized by exposure to 254 nm, 30 W of ultraviolet (UV) light for 6 h. The bioreactors based on different experimental design were inserted into chambers and transplanted to animals immediately after Plts attachment (Figure 2(a)).

All experiments were performed with the approval of the Nan Fang Hospital Institutional Animal Care and Use Committee. Each hemispheric polycarbonate chamber with an internal diameter of 2 cm and a volume of 2.00 mL was connected to a ring-like silicon sheet with or without pDA/GC/Plt or GC inside the chamber (Figure 2(a)). Sprague Dawley rats (280–300 g, n = 24, six in each group) were anesthetized by intraperitoneal injection of pentobarbital sodium (50 mg/kg). The chambers were inserted bilaterally as described in a previous study[10]. Briefly, a transverse incision was made in the groin to reveal the bilateral groin fat pad, which was then anchored to the adjacent muscle fascia with a 10/0 nylon suture. A chamber was placed and fixed in the space created between the skin and the fat pad. Two identical chambers were implanted in each rat. The silicon sheet with a hole of 1 cm in diameter in the center created an open chamber abutting the surrounding epigastric fat pad, thus providing contact with native adipose tissue.

A drug delivery system based on physical absorption of gelatin was employed in our previous research, the utilization of PRP directly exhibited more remarkable angiogenic effect compared to the physical absorption even the PRP would release the growth factors bristly after activation in vivo immediately rather than slow-releasing.[31] In order to verify the enhanced Plts immobilization with pDA assistance compared with direct PRP utilization, the rats were divided into four experimental groups depending on the contents of the chamber. Rats in the control group received blank chambers; in the PRP group, chambers were injected with 1 mL of PRP immediately after chamber placement; in the GC group, chambers contained GC without PRP; and in the pDA/GC/Plt group, chambers contained pDA/GC/Plt compounds. The rats were sacrificed at 4 and 12 weeks after TEC implantation (n = 3 per time point per group), and the implanted chambers and their contents were harvested and weighted.

Assessment of growth factors in chamber fluid

Fluid was extracted from implanted chambers using a 1-mL syringe on days 3, 7, 10, and 15. Levels of PDGF and VEGF were evaluated in the TEC fluid with ELISA using PDGF and VEGF ELISA kits (R&D Systems, Minneapolis, MN, USA) following the manufacturer's instructions.

Morphologic assessment of neoformed tissue by SEM

Four-week samples were fixed with 2% glutaraldehyde in 0.1M phosphate buffer, post-fixed in 1% osmium tetroxide in the same buffer for 1 h, dehydrated in increasing concentrations of acetone, and critical-point dried. Stubs were fixed to the samples with colloidal silver, and the samples were sputtered with gold using a MED 010 coater and examined with an S-3000N scanning electron microscope (Hitachi Company, Tokyo, Japan).

Whole mount staining

Fresh 12-week tissue samples from engineered adipose tissue and normal adipose tissue were stained following a reported method. Briefly, 1-mm sections of adipose tissue were incubated for 30 min at 37°C with Alexa Fluor 568–conjugated BODIPY and 647–conjugated lectin (Life Technologies, Thermo Fisher Scientific Inc., MA, USA) targeting adipocytes and vascular endothelial cells, whereas Hoechst 33342 (Dojindo, Dojindo Molecular Technologies, Inc., MD, USA) was used to stain the nuclei. Washed samples were examined with a confocal microscope (Olympus, Tokyo, Japan).

Histology and immunofluorescent staining

The samples were embedded in paraffin, sectioned, and stained with hematoxylin and eosin (H&E) and Masson trichrome (MT). Staining was performed according to standard protocol. Different sections were examined under a light microscope (Olympus BX51, Tokyo, Japan) and evaluated. For quantification of fibrosis, blue areas of sequential MT-stained fibrosis tissue were measured using ImageJ.

Immunofluorescent staining of 5-μm-thick sections of the harvested tissue samples was performed with the

following primary antibodies: Guinea pig anti-rat perilipin (dilution, 1:200; PROGEN Biotechnik GmbH, Heidelberg, Germany), rabbit anti-rat CD206 (dilution, 1:200; Abcam), rabbit anti-rat Ki67 (dilution, 1:200; Abcam plc., Toronto, Canada), and rabbit anti-mouse CD31 (dilution, 1:100; Novus Biologicals, Oakville, Canada). For double fluorescence staining, the following secondary antibodies were used: Alexa Fluor 488–conjugated goat anti-Guinea pig immunoglobulin G (dilution, 1:200; Abcam) and Alexa Fluor Rhodamine–conjugated chicken anti-rabbit immunoglobulin G (dilution, 1:200; Invitrogen). Isotype immunoglobulin G was used as a negative control for each immunostaining. Nuclei were stained with DAPI (dilution, 1:200; Sigma, St. Louis, MO, USA). The number of blood vessels was counted in 10 fields per slide (40× magnification) by two individuals. To quantify the proliferation rate, Ki67-positive cells were counted using ImageJ. CD206-positive cells were counted in the same way.

Results and discussion

Mechanical feature of GC scaffolds

GC and gelatin-MA hydrogel (referred to as "RT-GelMA") was synthesized through the free radical copolymerization of gelatin-MA at −20°C or room temperature, respectively. To determine the effect of temperature and concentration on the mechanical properties, uniaxial compression and rheology tests were performed. Generally, the modulus increased with the increasing concentration for cryogels. The RT-GelMA formed at room temperature displayed a rapid increase in the elastic modulus at relative large compressive strain (>35%), in contrast, the cryogels showed a gradual increase in the modulus prior to failure (Figure 2(b)). Moreover, the RT-GelMA exhibited around 62.8% of compressive deformation, but cryogels up to 76.5% (Figure 2(b)). An appropriate stiffness of extracellular matrix (ECM) is required for a pre-determined cell differentiation and tissue regeneration.[32,33] For instance, adipogenic markers can be significantly upregulated on a gel with a similar stiffness of 2 kPa to the native fat tissue.[11] In this study, Young's modulus was tuned (Figure 2(c)) and we found Young's modulus of 5% GC as 2.3 ± 1.2 kPa, which was similar to the native stiffness of subcutaneous fat tissue as previously reported (ca. 2–3 kPa).[34] The strain amplitude sweep tests for storage modulus were presented in Figure 2(d). The GC at 5% concentration exhibited storage modulus around 1 kPa and linear viscoelastic behavior at low strain (up to 0.4%), which were similar to normal adipose tissue rheological response.[35] Considering this, we used mechanical properties of 5% GC in the following studies.

The chemical structure of pristine gelatin, gelatin-MA, and pDA/GC were characterized by ATR spectroscopy, and the spectra were shown in Figure S1. The typical absorption bands around 3270–3370, 2928, 1640, and 1240 cm^{-1} were assigned to N–H stretching of amide I, C–H stretching of CH_2 group, stretch of C=O from amide I, and N–H bending of amide III, respectively, which revealed the backbone structure of gelatin. The intensity of the amide I was increased to some extent after methacrylate modification due to the contribution of C=C stretching (1680–1620 cm^{-1}). In addition, a new band around 970 cm^{-1} was distributed to the C–H stretching of C=C bonds with methacrylation, which further indicated the successful methacrylate groups introduction into free amino groups of gelatin. After a pDA modification, the absorption peaks at 2923 and 1064 cm^{-1} were attributed to the asymmetrical stretching vibrations of $–CH_3$ group and –COO group from long alkyl chains of polydopamine, respectively.

The morphology of GC with varied concentration, RT-GelMA, pDA/GC, and pDA/GC/Plt were observed by scanning electron microscopy (SEM), the interconnected porosity of the cryogel and RT-GelMA samples were further analyzed by water replacement method with slight modifications,[29,30] and the results were illustrated in Figures 3 and S2. As shown in the SEM images, the cross section of RT-GelMA and cryogels exhibited highly uniform and interconnected pore structure. The pore size and porosity of the cryogel and hydrogels varied as a function of the monomer concentration as well as fabrication temperature. The average pore size decreased significantly from 203.5 to 172.6 μm with increase in the concentration of gelatin-MA from 2% to 5%, meanwhile the porosity decreased slightly from $94.7 \pm 4.5\%$ to $90.2 \pm 3.2\%$. The fabrication temperature also affected interconnected porous architecture, and hydrogel made at room temperature exhibited smaller pore size than cryogel with same concentration, which decreased to 85.7 ± 22.4 μm, as well as the porosity ($90.2 \pm 3.2\%$ and $74.3 \pm 5.1\%$). It is worth pointing out that the formation of macrostructure in cryogel was determined by the competition between the rate of ice crystals nucleation and the polymerization speed, more intense nucleation and more ice crystals appeared on the top rather than bottom during the cooling process due to the lower density of ice compared to liquid, yielding a different pore structure at the bottom (Figure S2), where much smaller pore size was formed; however, this heterogeneous structure could be minimized through faster cooling to −20°C.[36] Clearly, the porous structure performance could be turned by controlling the monomer concentration or the gelation temperature. After immersion in PRP, the pDA/GC scaffold maintained its porous frame structure, but the porous interior was occupied by Plts with varied active states (Figure 3(c) and (d)).

Quantitative analysis of Plt levels in whole blood, PRP, and scaffolds

Plt concentration in PRP was significantly (fourfold) higher than that in whole blood ($2749 \pm 155.7 \times 10^9$/L vs $680 \pm 18.32 \times 10^9$/L). The level of immobilized Plts of the pDA/GC/Plt scaffold was significantly higher than that of

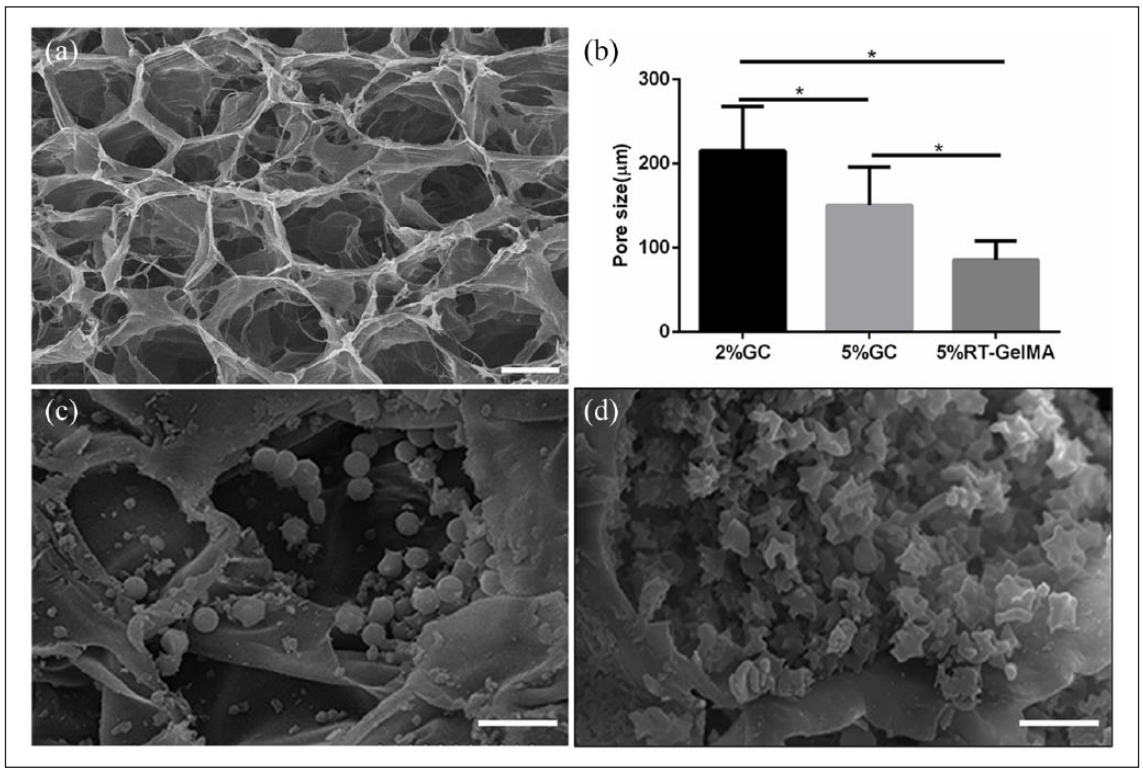

Figure 3. Representative SEM porous structure of 5% GC (a, scale bar = 100 μm) and pore size of 2% GC, 5% GC, and 5% RT-GelMA (b) were shown. In the process of Plt immobilization, different forms of Plts attached to the scaffold, including Plts in the non-activated (c) and activated states (d), scale bar = 10 μm.

the GC/Plt scaffold ($2416 \pm 205.1 \times 10^9$/L vs $882 \pm 75.16 \times 10^9$/L, $p < 0.05$). There was no significant difference in Plt concentration between the PRP and pDA/GC/Plt groups ($2749 \pm 155.7 \times 10^9$/L vs $2416 \pm 205.1 \times 10^9$/L, $p > 0.05$). pDA coating resulted in a 2.7-fold increase in the number of Plts immobilized on the GC scaffold (Figure 4). pDA-coated GC immobilized nearly three times the number of Plts immobilized by GC alone, which demonstrated the efficiency of pDA-mediated surface modification. Adhesion of Plts onto the bare GC is mediated by a physical interaction (30); besides the non-specific physical absorption, a stronger and more stable covalent crosslinking between Plts and pDA film occurred at pDA group.

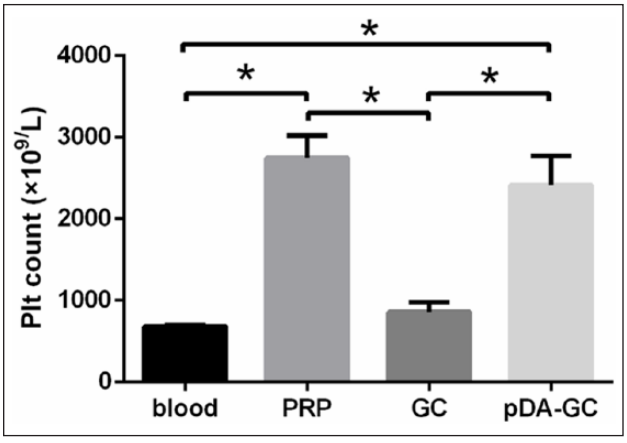

Figure 4. Plt concentrations in four systems. All three processing methods significantly increased Plt concentration compared with that in whole blood (blood: $680 \pm 18.32 \times 10^9$/L; Plt-rich plasma (PRP): $2749 \pm 155.7 \times 10^9$/L; gelatin cryogel (GC): $882 \pm 75.16 \times 10^9$/L; and polydopamine (pDA)/GC/Plt: $2416 \pm 205.1 \times 10^9$/L). The pDA/GC/Plt group had a significantly higher Plt concentration than the GC group ($p < 0.05$). There was no difference between the PRP and pDA/GC/Plt groups ($p > 0.05$).

Cytotoxicity and cell proliferation

CCK-8 assays (Figure 5) revealed no significant differences between the control, GC, and pDA/GC groups at any tested time point ($p > 0.05$), while pDA/GC/Plt significantly improved cell growth after 12 h of incubation ($p < 0.05$). The results suggested that GC or pDA/GC had great biocompatibility and pDA/GC/Plt improved the proliferation of ASCs.

In vitro growth factor release

The growth factor release pattern of pDA/GC/Plt was tested with ELISA. After an initial burst, the release of PDGF gradually decreased over time in both groups (Figure 6(a)). PDGF in the PRP group could not be detected after 24 h, while that in the pDA/GC/Plt group could still be detected

for at least 72 h. A significant difference in PDGF concentration between these two groups was observed after 6 h ($p < 0.05$). The release of VEGF reached its peak at 6 h in the PRP group and 12 h in the pDA/GC/Plt group, which showed a delayed peak of release due to Plt immobilization (Figure 6(b)). After 6 h, the VEGF level decreased dramatically in the PRP group, remained low for the following 48 h, and could not be detected after 72 h. In contrast, in the pDA/GC/Plt group, a sustained release was observed after the peak, with a relatively high VEGF level maintained for up to at least 72 h. A significant difference in VEGF concentration between these two groups was present after 6 h ($p < 0.05$). At least seven fundamental growth factor proteins exist within α-granules.[16] VEGF and PDGF are two of the important factors crucial for angiogenesis. VEGF promotes endothelial cell proliferation,[37] while PDGF can help stabilize the vessel and improve its maturation through recruitment and proliferation of mural cells.[38,39] Given the short half-life of VEGF, in a chamber model, it is expected to act by promoting the establishment of an initial vascular network at the stage of early recruitment and proliferation of endothelial cells, mural cells, or their precursors.[40] PDGF may also recruit cells such as inflammatory cells and adipocytes to the periphery of the capillaries.[41,42] Growth factor releasing profiles indicated a higher and sustained release with pDA assistance.

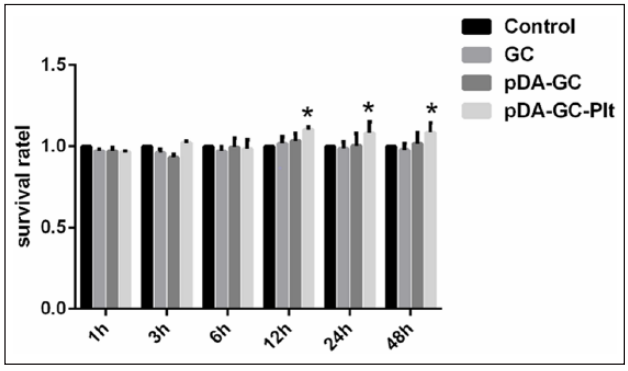

Figure 5. CCK-8 assay of adipose stem cells (ASCs) seeded on different scaffolds. No significant differences between the GC, pDA/GC, and control groups, pDA/GC/Plt scaffold significantly improved ASCs proliferation ($p < 0.05$).

In vivo results

Growth factors in chamber fluid. VEGF and PDGF were two important growth factors associated with angiogenesis and subsequent tissue regeneration. We tested the growth factor levels from the chamber fluid. The PDGF level significantly increased after day 7 in the pDA/GC/Plt group compared with the other two groups ($p < 0.05$) (Figure 6(c)). The VEGF level in the pDA/GC/Plt group increased significantly in the first 3 days compared with that of the other two groups ($p < 0.05$), which might be attributable to the immobilized Plts. Around day 15, the VEGF level was still significantly higher in the pDA/GC/Plt group than in the other two groups ($p < 0.05$), which might be caused by

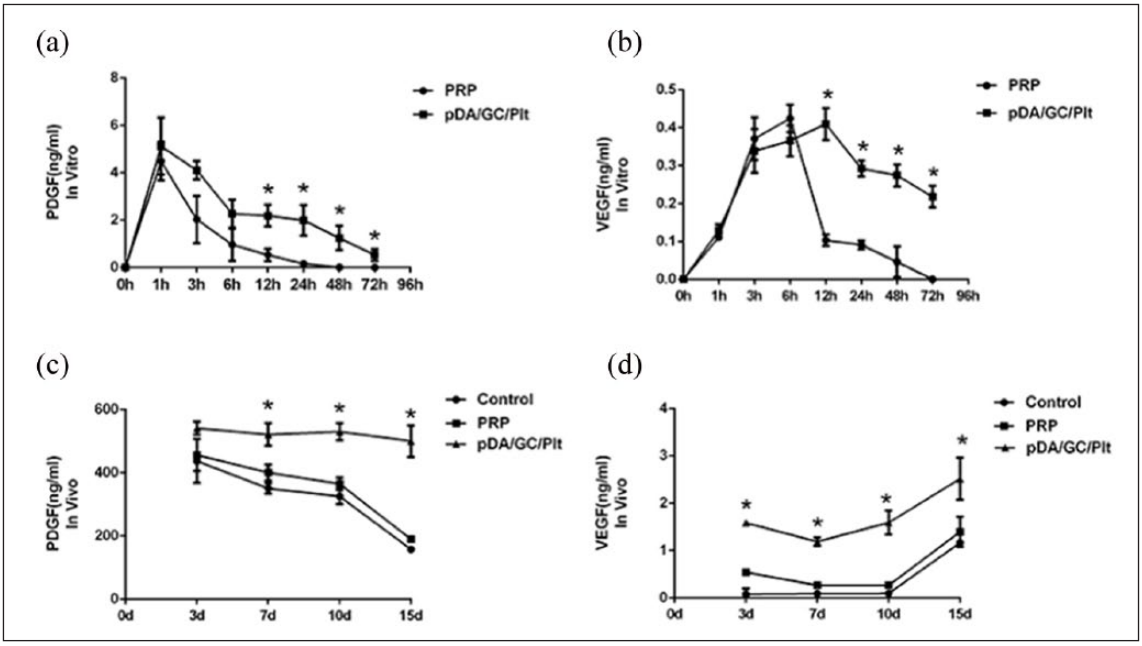

Figure 6. Growth factors release by the pDA/GC/Plt system. PDGF (a) and VEGF (b) were detected with ELISA. The release was prolonged in the pDA/GC/Plt group compared to that in the PRP group. A significant difference was observed after 3 h for both PDGF and VEGF. Chamber fluid was extracted and tested by ELISA for PDGF (c) and VEGF (d). pDA/GC/Plt incorporated into the TEC had significantly higher levels of PDGF and VEGF from days 7 and 3, respectively ($p < 0.05$).

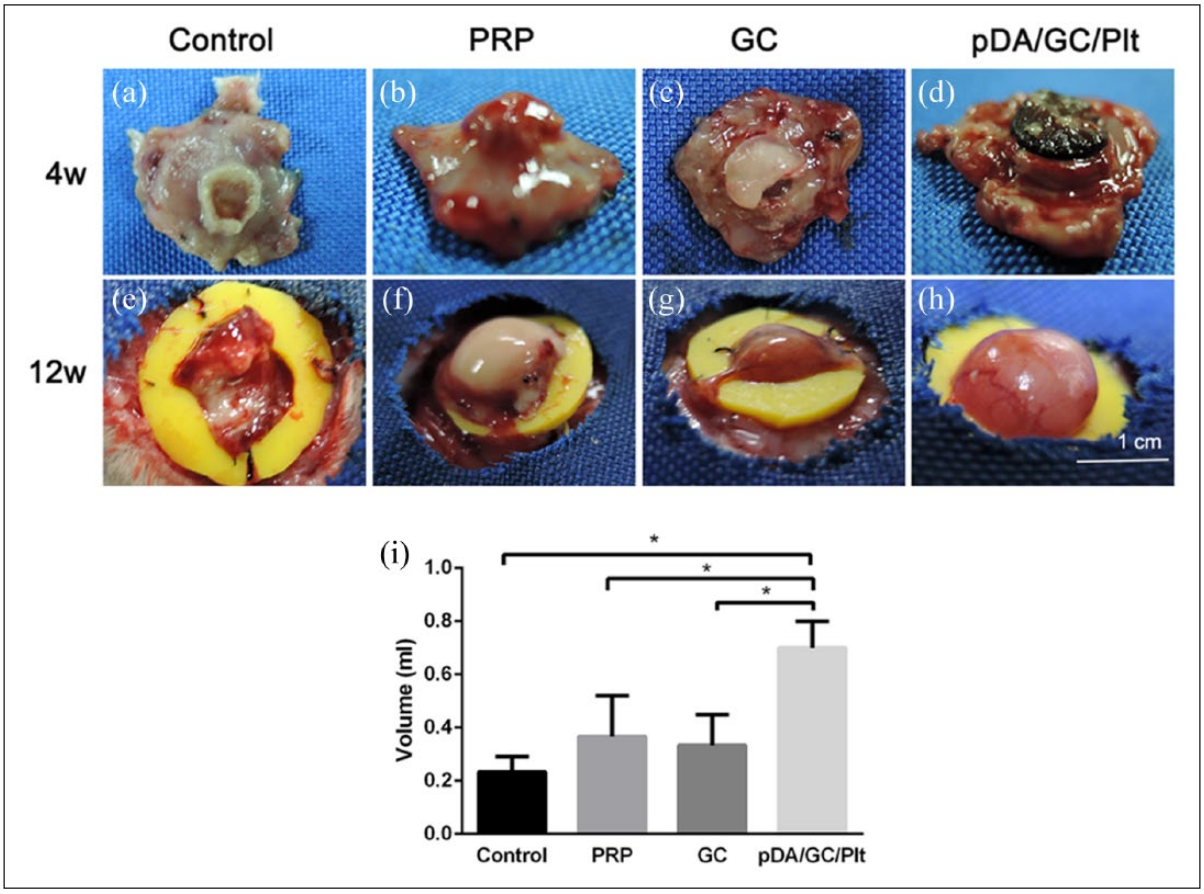

Figure 7. Whole constructs. Photographs of representative chamber tissue constructs harvested at 4 weeks (a: control, b: PRP, c: GC, d: pDA/GC/Plt) and 12 weeks (e: control, f: PRP, g: GC, h: pDA/GC/Plt). Tissue volumes in the 4 experimental groups at 12 weeks: control, 0.23 ± 0.05 mL; PRP, 0.36 ± 0.15 mL; GC, 0.33 ± 0.11 mL; pDA/GC/Plt, 0.70 ± 0.10 mL (i).

more efficient recruitment of stem cells and inflammatory cells to this bioreactor system (Figure 6(d)). However, the PRP group showed no differences in PDGF and VEGF levels from the control group at any time point ($p > 0.05$).

Macroscopic construct appearance and total tissue volume. Gross examination at week 4 revealed that tissue from the fat pad had grown into the chamber and around the GC scaffold in the pDA/GC/Plt (Figure 7(d)) and GC (Figure 7(c)) groups, while in the PRP (Figure 7(b)) and control (Figure 7(a)) groups without a GC scaffold, a smaller, raised tissue from the fat pad was growing into the chamber through the ring-like silicon sheet hole. At week 12, the newly generated adipose tissue showed further growth and no GC residue could be found (Figure 7(e)–(h)). The volume of the newly generated adipose tissue in the 12-week samples was determined by fluid displacement (Figure 7(i)). The pDA/GC/Plt group had significantly more newly generated adipose tissue than the other three groups ($p < 0.05$).

Confirmation of tissue incorporation into the biomaterial. SEM results revealed co-existence and interaction of GC and local tissue (Figure 8(a)). By week 4, the GC had degraded, and parts of its porous-like structure had collapsed (Figure 8(b)). Along with the degradation of the GC scaffold, host cells (Figure 8(c)) migrated into the provided scaffold and began to secrete fibrous protein to form a natural fiber network (Figure 8(d)), which was incorporated into the GC scaffold. With the degradation of GC and secretion of fiber from recruited cells, a natural ECM scaffold formed and replaced the synthetic one. In addition, some activated Plts were still detected in the scaffold structure (Figure 8(e)), which might contribute to functional cell recruitment and fibrin network formation.

Visualization of tissue architecture in engineered adipose tissue. To visualize the tissue architecture and demonstrate adipocyte and blood vessel interaction in the coherent tissue formed in the pDA/GC/Plt scaffold in vivo, the 12-week samples were subjected to whole mount staining (Figure 9). The de novo–formed fat tissue showed structural resemblance to native fat tissue (Figure 9(a)). The BODIPY−/DAPI+ field might be composed of fibrous tissue, which separated adipose tissue lobules. These stain-negative areas might be residual GC. The lectin-positive blood vessels

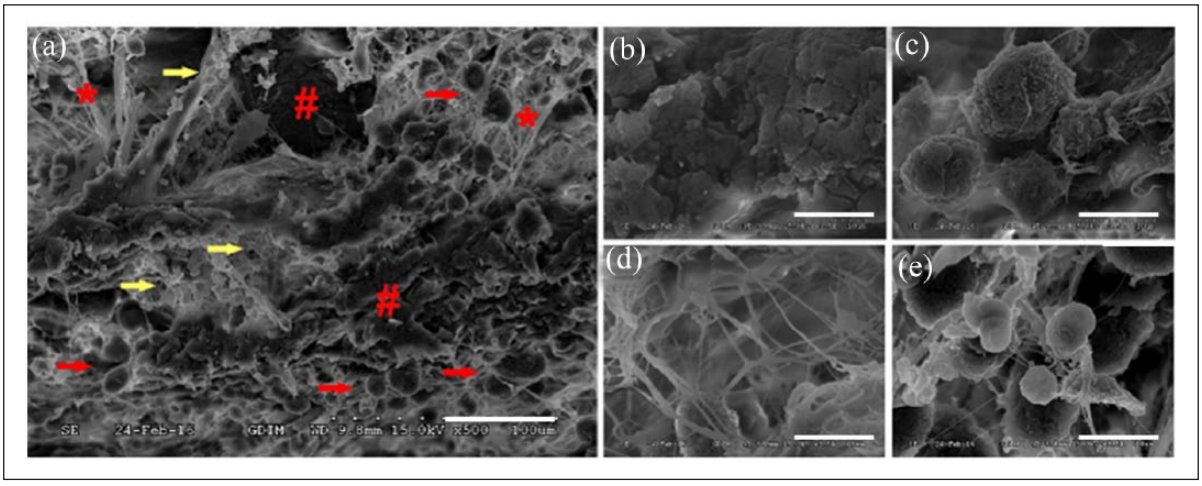

Figure 8. Scanning electron microscopy (SEM) revealed that the GC and the local tissue co-existed and interacted at week 4 (a, scale bar = 50 μm). The residual GC scaffold (red pound sign) and the fibrin network (red asterisks) secreted by infiltrated cells (red arrows) were incorporated into each other. Some activated Plts were still detectable in the scaffold structure (yellow arrows). Close-up views of the fibrin network (b), resident cells (c), Plts (d), and residual GC scaffold (e), scale bar = 10 μm.

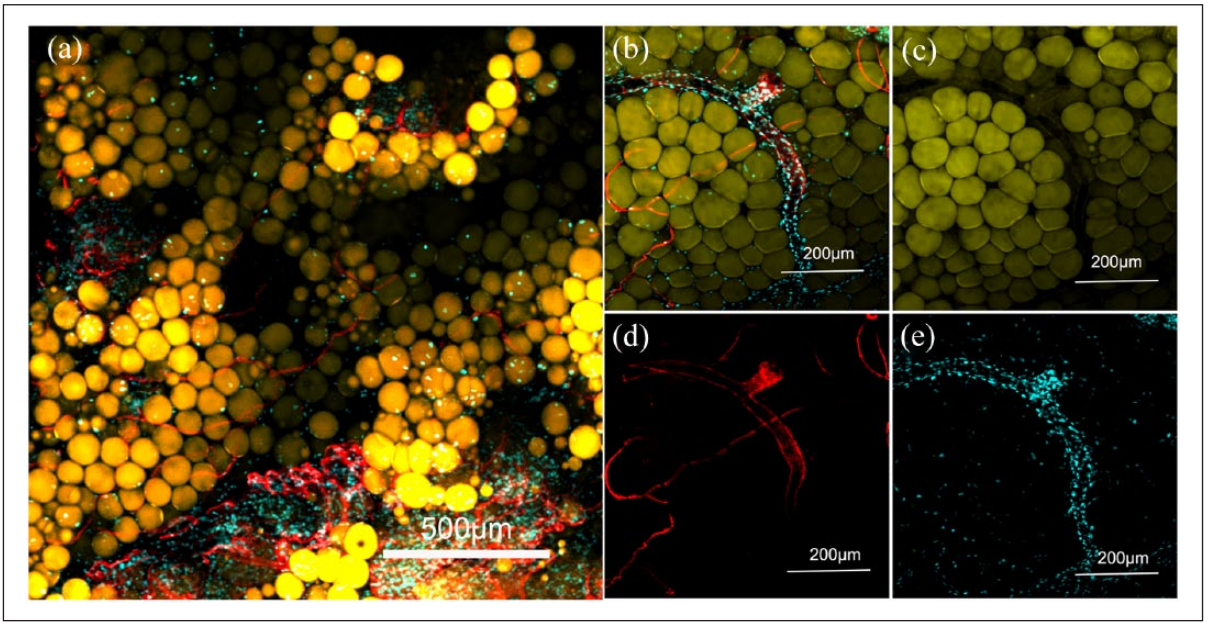

Figure 9. Whole mount staining of engineered adipose tissue from the pDA/GC/Plt group at 12 weeks. A group of natural but less densely packed adipocytes was observed (a). Adipocytes were stained with luminous yellow, vessels were stained with red, blue represented the nucleus. Whole mount staining showed that extensive vascularization was achieved, with large vessels incorporated into the adipose tissue (b). BODIPY staining shows the normal adipose structure (c). Lectin staining shows the abundant vessel structure (d). DAPI shows the nuclei (e).

assembled within the engineered fat tissue, surrounded by BODIPY-positive adipocytes. Not only were there lumens of small blood vessels but large vessels were also incorporated into the engineered adipose tissue (Figure 9(b)), demonstrating that a completely mature vascular system was established in the engineered fat tissue in this bioreactor.

Histological assessment of the newly generated adipose tissue. Histological analysis showed that, at week 4, the engineered tissue exhibited abundant, well-vascularized connective tissue in all four groups, with numerous inflammatory cells and a few small adipocytes around the vessels (Figure 10(a)–(d)). Blood vessels were quantified in all the groups (Figure 10(m)). The pDA/GC/Plt group had significantly more vessel lumens than the other three groups at 4 weeks, which indicated that more capillaries were formed within the bioreactor. By week 12, most of the vascularized connective tissue in the flaps had been

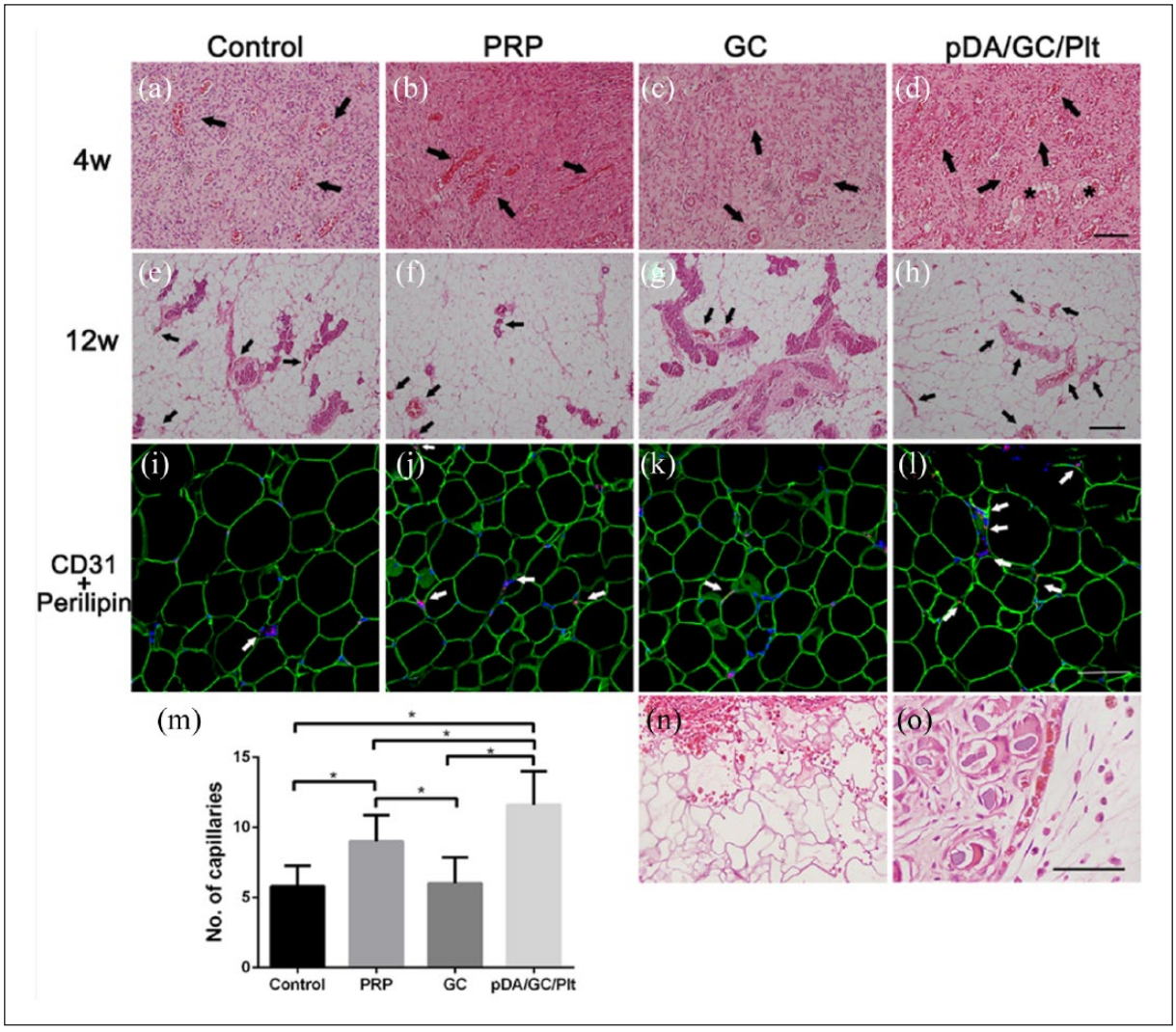

Figure 10. Histological analysis of regenerative adipose tissue at week 4 (a: control, b: PRP, c: GC, d: pDA/GC/Plt) and week 12 (e: control, f: PRP, g: GC, h: pDA/GC/Plt). Black arrows show the vascular connective tissue, asterisk represent the small adipocytes. Scale bar = 0.1 mm. CD31 staining of the control (i), PRP (j), GC (k), and pDA/GC/Plt (l) groups showed vessel density at week 12. Red denoted the CD31-positive cells, green denoted the adipocytes, and blue denoted the nuclear. Scale bar = 0.1 mm. Vessel density was evaluated in week 4 samples (m,*$p < 0.05$). A relatively intact porous structure of GC was observed in pDA/GC/Plt group at 4 weeks (n) (scale bar = 0.1 mm), while only GC debris was found in pDA/GC/Plt group at 12 weeks (o) (thin arrow, scale bar = 0.5 mm).

replaced by mature adipocytes with well-developed vascular system (Figure 10(e)–(h)). The pDA/GC/Plt group had more numerous and larger blood vessels and mature adipocytes.

We observed a relatively intact porous structure of the GC scaffold at week 4 (Figure 10(n)). Some of the GC had degraded into debris and was surrounded by layers of inflammatory cells (Figure 10(o)). At week 12, no materials or debris were found. Early after implantation, mesenchymal cells migrate into the GC scaffold, where they can proliferate and differentiate, as illustrated in SEM and H&E staining results. During this process, migratory cells secrete fibrous protein to construct a natural ECM network. By week 4, GC had partially degraded, and its porous structure had begun to collapse. It was completely disintegrated at 12 weeks. Eventually, a natural ECM replaced the temporary GC scaffold. Therefore, the formation and maturation of the natural ECM were accompanied by gradual disintegration of the extraneous gelatin serving as a scaffold, permitting the formation of naturally engineered adipose tissue.

The 12-week samples were stained with CD31 immunofluorescent stain to identify angiogenesis and microvascular ingrowth inside the engineered adipose tissue (Figure 10(i)–(l)). Consistent with the results of H&E staining, there were more CD31-positive vessels in the pDA/GC/Plt group than in the other three groups.

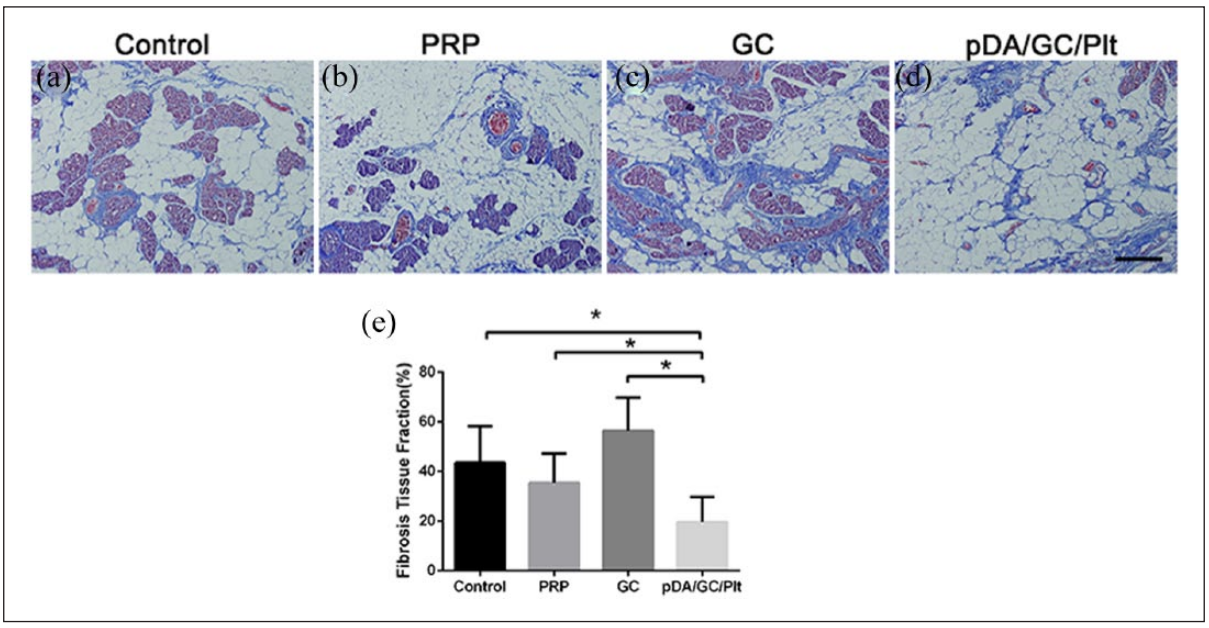

Figure 11. Masson staining of week 12 samples of chamber tissues from the control group (a), PRP group (b), GC group (c), and pDA/GC/Plt group (d). Scale bar = 0.1 mm. Statistical evaluation of fibrosis area in the four groups: control: 42.80% ± 12.380%; PRP: 35.40% ± 11.983%; GC: 56.40% ± 13.39%; and pDA/GC/Plt: 19.20% ± 9.338% (e).

In terms of fibrosis (Figure 11), Masson staining of the 12 week samples showed a significantly higher proportion of fibrosis in the GC group than in any other group ($p < 0.05$), while pDA/GC/Plt group had the least fibrosis ($p < 0.05$).

Proliferation assessment. Cellular proliferation inside the engineered adipose tissue was assessed using Ki67 and perilipin immunofluorescent staining (Figure 12). At week 4, Ki67-positive cells (red) took up a large proportion of DAPI-positive cells, which indicated a state of extraordinarily active cellular proliferation in all four TEC models (Figure 12(a)–(d)). Ki67-positive cell count revealed that the pDA/GC/Plt group had a significantly higher proportion of proliferating cells than the other three groups ($p < 0.05$, Figure 12(i)), which showed no significant differences ($p > 0.05$). At week 12, as fat lobules formed, the numbers of Ki67-positive cells decreased dramatically. Few Ki67-positive cells were observed among the adipocytes (Figure 12(e)–(h)). Many cellular components in the TEC chamber participated in the early stage of tissue regeneration, including inflammatory cells, adipose stem cells, and bone-derived stem cells. We observed more Ki67-positive cells in the pDA/GC/Plt group, which had more active cellular proliferation.

Macrophage infiltration. The constructs were stained with perilipin and CD206 to evaluate macrophage infiltration (Figure 13). At week 4, numerous CD206-positive macrophages appeared in all four groups (Figure 13(a)–(d)). The pDA/GC/Plt and GC groups had significantly more CD206-positive cells than the PRP and control groups ($p < 0.05$, Figure 13(i)). At week 12, in all four groups of engineered adipose tissue, CD206-positive macrophages were mainly located in the perilipin-negative area, which might be a fibrosis area (Figure 13(e)–(h)). The CD206-positive cell count revealed that the GC group had a significantly higher level of macrophages than the other three groups ($p < 0.05$), and there was no significant difference between the pDA/GC/Plt and control groups ($p > 0.05$, Figure 13(i)). Plt activation is considered to be upstream of the cascade of inflammation.[43–45] In different regeneration models, inflammation-induced regeneration is the core of tissue repair. Activated Plts and Plt-derived proteins can bind to leukocytes and modulate leukocyte functions, contributing to inflammatory and immune responses.[46–49] Plt and/or neutrophil interactions with monocytes facilitate their recruitment and differentiation into macrophages, modulate cytokine release, and regulate macrophage functions. In particular, CD206-positive M2 macrophages play a crucial part in angiogenesis, ECM remodeling, and stem cell regulation to influence tissue regeneration.[46–49] Furthermore, depletion of macrophages in chamber dramatically inhibited tissue growth, which demonstrates a strong impact of inflammation in tissue regeneration in chamber.[50] In this study, we employed a Plt immobilization system to facilitate the triggering of inflammation. As a result, more CD206-positive macrophages were recruited in the pDA/GC/Plt group at week 4, leading to a positive effect on tissue regeneration at the early stage. At week 12, the GC group still had more CD206-positive cells than the other three groups, while the level of macrophages in the

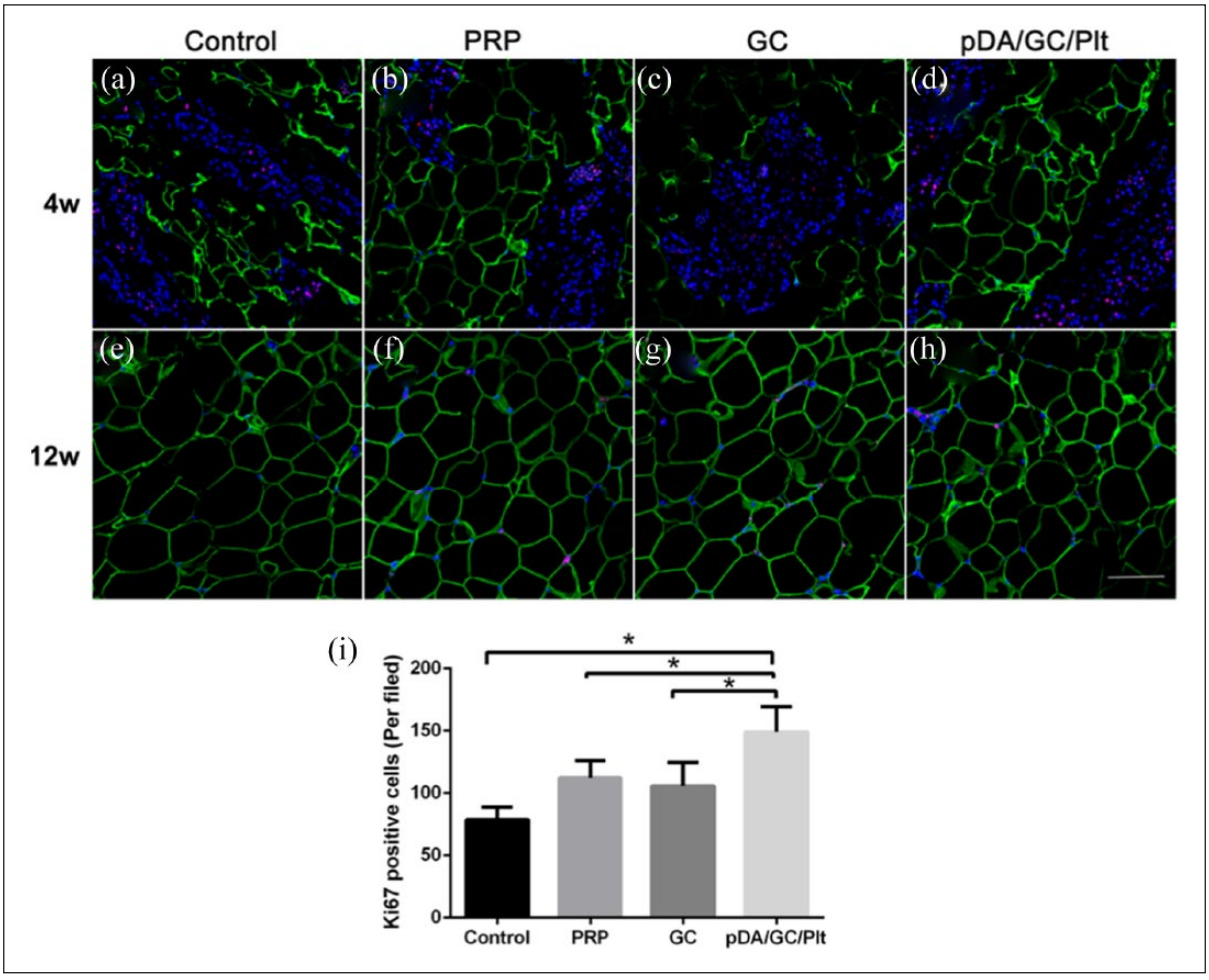

Figure 12. Ki67 and perilipin double staining of sections of chamber tissue at 4 weeks (a: control, b: PRP, c: GC, d: pDA/GC/Plt) and 12 weeks (e: control, f: PRP, g: GC, h: pDA/GC/Plt). Red denoted the ki67-positive cells, green denoted the adipocytes, and blue denoted the nuclear. Scale bar = 0.1 mm. Quantification of Ki67-positive cells in all groups at 4 weeks (i).

pDA/GC/Plt decreased and approached that of the control group. Fibrosis, which might be caused by hypoxia or unspecific foreign body reaction inducing by external biomaterials implantation, is associated with long-term presence of CD206-positive macrophages.[51,52] During the adipose tissue regeneration in chamber model, the inflammatory exudation resulted by the silicone chamber implantation and interruption of fat tissue integrity would resemble to a "self-synthesized ECM" which acted as provisional niche for proliferation and differentiation of precursor cells, macrophages decreased over time with the blood supply reconstruction because no external factor affected the natural growth process.[25] The vascularization of GC group was slightly less than control group but significantly less than PRP and pDA/GC/Plt group after 12 weeks (Figure S3), and this phenomenon could be explained by the unspecific foreign body reaction which led to significant fibrous septum formation and following contraction to inner soft tissue; moreover, since GC does not exert a positive effect in angiogenesis, insufficient vascularization in the engineered adipose tissue might lead to local hypoxia and prolonged macrophages retention. Thus, we observed a higher macrophage infiltration level in the GC group at 12 weeks, which is consistent with the result that the GC group had the most severe fibrosis among all four groups. In contrast, the pDA/GC/Plt group had better vascularization and smaller area of hypoxia, which led to a lower level of macrophage infiltration and less fibrosis.

This study has some limitations that warrant attention. The degradation kinetics of GC in vivo and its effect to the vascularization and adipose tissue regeneration were not quantified in detail. Some evidence from macroscopical and histological analysis suggested GC could retain its structure after 4 weeks and partially degraded after 12 weeks at current study, which was similar to previous reports.[28,53] Moreover, our previous study revealed the efficiency of physical absorption of Plts to gelatin was insufficient, which resulted to unsatisfactory growth factors release as well as vascularization and survival of adipose tissue transplantation compared

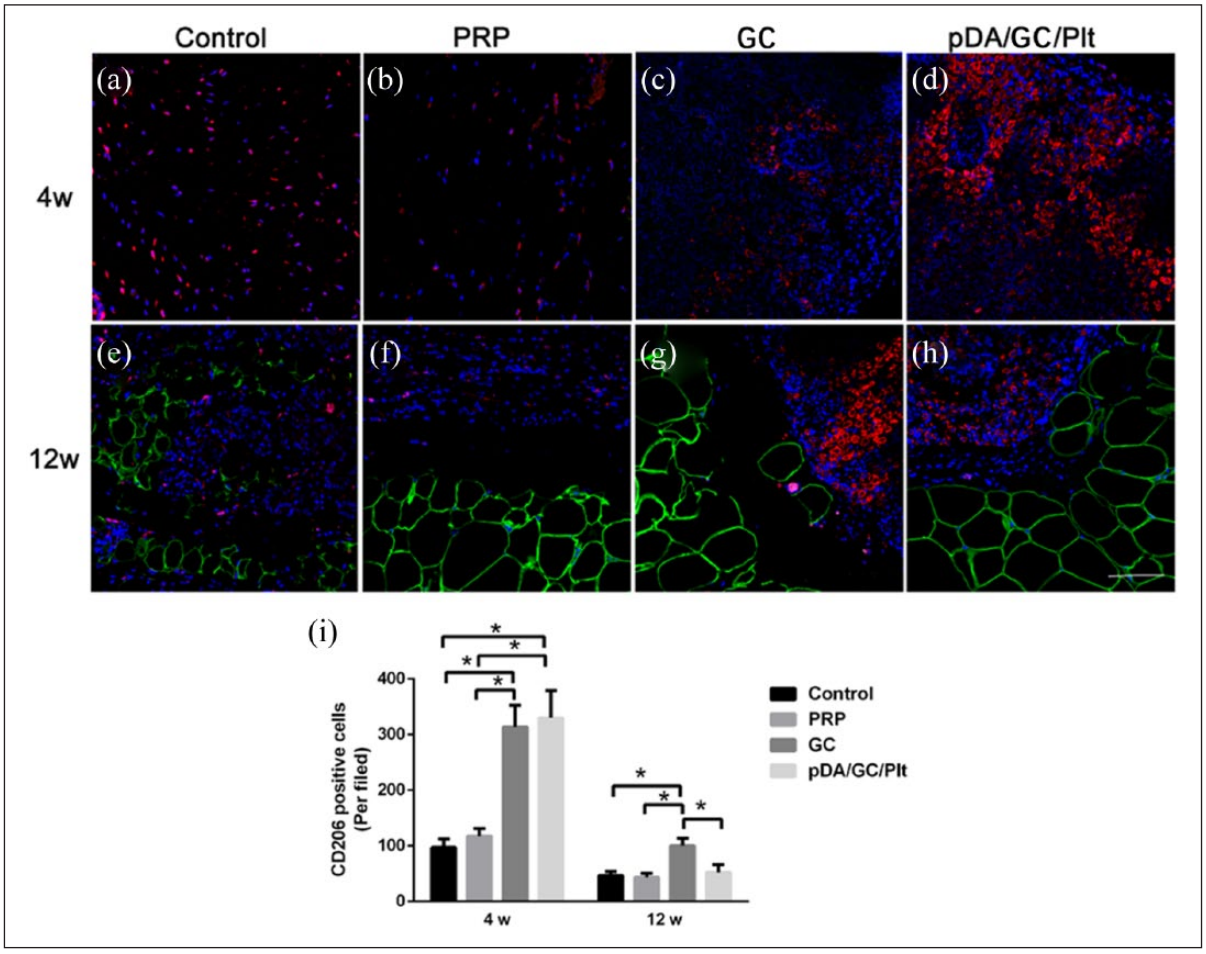

Figure 13. CD206 and perilipin double staining of sections of chamber tissue at 4 weeks (a: control, b: PRP, c: GC, d: pDA/GC/Plt) and 12 weeks (e: control, f: PRP, g: GC, h: pDA/GC/Plt). Red denoted the CD206-positive cells, green denoted the adipocytes, and blue denoted the nuclear. Scale bar = 0.1 mm. Quantification of CD206-positive cells was shown for all four groups at 4 weeks and at 12 weeks (i).

with PRP injection;[31] however, liquid PRP solution would lead to burst release of growth factor after activation in vivo immediately; taking into consideration of various elements, we used GC as a carrier, in combination with pDA-assisted Plts immobilization, as a delivery system to enhance the absorption efficiency in this study to make up the shortage of direct utilization of PRP. Future studies will explore efficiency of different drug delivery systems in more various regenerative models.

Statistical analysis

Data were expressed as means ± standard error. The results were analyzed with repeated analysis of variance. Independent Student's t-test (two groups at a single time point) and one-way analysis of variance (more than two groups at a single time point) were performed. A value of $p < 0.05$ was considered to indicate a statistically significant difference.

Conclusion

In this study, we introduced a guided adipose tissue regeneration strategy to regenerate large adipose tissue. We first fabricated an elastic gelatin gel (5%) with Young's modulus 2.3 ± 1.2 kPa, mimicking fat tissue (2–3 kPa). The mussel adhesive–inspired surface coating promoted the immobilization of Plts to GC, and this Plt-enriched GC displayed higher and sustained growth factor release for sufficient and rapid vascularization and recruiting more precursor cells for adipose tissue regeneration, which resulted in formation of a large volume of adipose tissue in our minimally invasive chamber model.

Acknowledgements

M.X. thanks the National Science and Engineering Research Council of Canada (NSERC) Discovery Grant and NSERC Discovery Accelerator Supplements Award. Q.C. and J.C. contributed equally to this work.

Declaration of conflicting interests

The author(s) declared no potential conflicts of interest with respect to the research, authorship, and/or publication of this article.

Funding

The author(s) disclosed receipt of the following financial support for the research, authorship and/or publication of this article: This work was supported by the National Nature Science Foundation of China (81671931 and 81701920).

Supplemental Material

Supplemental material is available for this article online.

References

1. Choi JH, Gimble JM, Lee K, et al. Adipose tissue engineering for soft tissue regeneration. *Tissue Eng Part B Rev* 2010; 16: 413–426.
2. Sterodimas A, De Faria J, Correa WE, et al. Tissue engineering in plastic surgery: an up-to-date review of the current literature. *Ann Plast Surg* 2009; 62: 97–103.
3. Casadei A, Epis R, Ferroni L, et al. Adipose tissue regeneration: a state of the art. *Biomed Res Int* 2012; 2012: 462543.
4. Mian R, Morrison WA, Hurley JV, et al. Formation of new tissue from an arteriovenous loop in the absence of added extracellular matrix. *Tissue Eng* 2000; 6: 595–603.
5. Dolderer JH, Abberton KM, Thompson EW, et al. Spontaneous large volume adipose tissue generation from a vascularized pedicled fat flap inside a chamber space. *Tissue Eng* 2007; 13: 673–681.
6. Hofer S, Knight KM, Cooper-White JJ, et al. Increasing the volume of vascularized tissue formation in engineered constructs: an experimental study in rats. *Plast Reconstr Surg* 2003; 111: 1186–1192; discussion 1193–1194.
7. Morrison WA, Marre D, Grinsell D, et al. Creation of a large adipose tissue construct in humans using a tissue-engineering chamber: a step forward in the clinical application of soft tissue engineering. *EBioMedicine* 2016; 6: 238–245.
8. D'arpa S, Cordova A, Pignatti M, et al. Freestyle pedicled perforator flaps: safety, prevention of complications, and management based on 85 consecutive cases. *Plast Reconstr Surg* 2011; 128: 892–906.
9. Miller KD, Siegel RL, Lin CC, et al. Cancer treatment and survivorship statistics, 2016. *CA Cancer J Clin* 2016; 66: 271–289.
10. Peng Z, Dong Z, Chang Q, et al. Tissue engineering chamber promotes adipose tissue regeneration in adipose tissue engineering models through induced aseptic inflammation. *Tissue Eng Part C Methods* 2014; 20: 875–885.
11. Young DA, Choi YS, Engler AJ, et al. Stimulation of adipogenesis of adult adipose-derived stem cells using substrates that mimic the stiffness of adipose tissue. *Biomaterials* 2013; 34: 8581–8588.
12. Kuttappan S, Mathew D and Nair MB. Biomimetic composite scaffolds containing bioceramics and collagen/gelatin for bone tissue engineering—a mini review. *Int J Biol Macromol* 2016; 93: 1390–1401.
13. Singh D, Zo SM, Kumar A, et al. Engineering three-dimensional macroporous hydroxyethyl methacrylate-alginate-gelatin cryogel for growth and proliferation of lung epithelial cells. *J Biomater Sci Polym Ed* 2013; 24: 1343–1359.
14. Choi JS, Yang H-J, Kim BS, et al. Fabrication of porous extracellular matrix scaffolds from human adipose tissue. *Tissue Eng Part C Methods* 2009; 16: 387–396.
15. Mazzucco L, Medici D, Serra M, et al. The use of autologous platelet gel to treat difficult-to-heal wounds: a pilot study. *Transfusion* 2004; 44: 1013–1018.
16. Marx RE. Platelet-rich plasma (PRP): what is PRP and what is not PRP? *Implant Dent* 2001; 10: 225–228.
17. Marx RE, Carlson ER, Eichstaedt RM, et al. Platelet-rich plasma: growth factor enhancement for bone grafts. *Oral Surg Oral Med Oral Pathol Oral Radiol Endod* 1998; 85: 638–646.
18. Roubelakis MG, Trohatou O, Roubelakis A, et al. Platelet-rich plasma (PRP) promotes fetal mesenchymal stem/stromal cell migration and wound healing process. *Stem Cell Rev* 2014; 10: 417–428.
19. Lee H, Lee Y, Statz AR, et al. Substrate-independent layer-by-layer assembly by using mussel-adhesive-inspired polymers. *Adv Mater* 2008; 20: 1619–1623.
20. Yang K, Lee JS, Kim J, et al. Polydopamine-mediated surface modification of scaffold materials for human neural stem cell engineering. *Biomaterials* 2012; 33: 6952–6964.
21. Lee H, Dellatore SM, Miller WM, et al. Mussel-inspired surface chemistry for multifunctional coatings. *Science* 2007; 318: 426–430.
22. Ho C-C and Ding S-J. Structure, properties and applications of mussel-inspired polydopamine. *J Biomed Nanotechnol* 2014; 10: 3063–3084.
23. Cui J, Yan Y, Such GK, et al. Immobilization and intracellular delivery of an anticancer drug using mussel-inspired polydopamine capsules. *Biomacromolecules* 2012; 13: 2225–2228.
24. Black KC, Yi J, Rivera JG, et al. Polydopamine-enabled surface functionalization of gold nanorods for cancer cell-targeted imaging and photothermal therapy. *Nanomedicine* 2013; 8: 17–28.
25. Zhan W, Chang Q, Xiao X, et al. Self-synthesized extracellular matrix contributes to mature adipose tissue regeneration in a tissue engineering chamber. *Wound Repair Regen* 2015; 23: 443–452.
26. Wang H, Zhou L, Liao J, et al. Cell-laden photocrosslinked GelMA-DexMA copolymer hydrogels with tunable mechanical properties for tissue engineering. *J Mater Sci Mater Med* 2014; 25: 2173–2183.
27. De Cock LJ, De Wever O, Hammad H, et al. Engineered 3D microporous gelatin scaffolds to study cell migration. *Chem Commun* 2012; 48: 3512–3514.
28. Koshy ST, Ferrante TC, Lewin SA, et al. Injectable, porous, and cell-responsive gelatin cryogels. *Biomaterials* 2014; 35: 2477–2487.
29. Kim I, Lee SS, Bae S, et al. Heparin functionalized injectable cryogel with rapid shape-recovery property for neovascularization. *Biomacromolecules* 2018; 19: 2257–2269.
30. Bencherif SA, Sands RW, Bhatta D, et al. Injectable preformed scaffolds with shape-memory properties. *Proc Natl Acad Sci USA* 2012; 109: 19590–19595.

31. Zhou S, Chang Q, Lu F, et al. Injectable mussel-inspired immobilization of platelet-rich plasma on microspheres bridging adipose micro-tissues to improve autologous fat transplantation by controlling release of PDGF and VEGF, angiogenesis, stem cell migration. *Adv Healthc Mater* 2017; 6: 1700131.
32. Ting AC, Craft RO, Palmer JA, et al. The adipogenic potential of various extracellular matrices under the influence of an angiogenic growth factor combination in a mouse tissue engineering chamber. *Acta Biomater* 2014; 10: 1907–1918.
33. Hamid ZA, Blencowe A, Ozcelik B, et al. Epoxy-amine synthesised hydrogel scaffolds for soft-tissue engineering. *Biomaterials* 2010; 31: 6454–6467.
34. Samani A, Bishop J, Luginbuhl C, et al. Measuring the elastic modulus of ex vivo small tissue samples. *Phys Med Biol* 2003; 48: 2183–2198.
35. Schoemaker I, Hoefnagel PP, Mastenbroek TJ, et al. Elasticity, viscosity, and deformation of orbital fat. *Invest Ophthalmol Vis Sci* 2006; 47: 4819–4826.
36. Hwang YS, Zhang C and Varghese S. Poly(ethylene glycol) cryogels as potential cell scaffolds: effect of polymerization conditions on cryogel microstructure and properties. *J Mater Chem* 2010; 20: 345–351.
37. Ferrara N, Houck K, Jakeman L, et al. Molecular and biological properties of the vascular endothelial growth factor family of proteins. *Endocr Rev* 1992; 13: 18–32.
38. Darland DC and D'Amore PA. Blood vessel maturation: vascular development comes of age. *J Clin Invest* 1999; 103: 157–158.
39. Hirschi KK, Rohovsky SA, Beck LH, et al. Endothelial cells modulate the proliferation of mural cell precursors via platelet-derived growth factor-BB and heterotypic cell contact. *Circ Res* 1999; 84: 298–305.
40. Rophael JA, Craft RO, Palmer JA, et al. Angiogenic growth factor synergism in a murine tissue engineering model of angiogenesis and adipogenesis. *Am J Pathol* 2007; 171: 2048–2057.
41. Horikawa S, Ishii Y, Hamashima T, et al. PDGFRα plays a crucial role in connective tissue remodeling. *Sci Rep* 2015; 5: 17948.
42. Yang P, Manaenko A, Xu F, et al. Role of PDGF-D and PDGFR-β in neuroinflammation in experimental ICH mice model. *Exp Neurol* 2016; 283: 157–164.
43. Kral JB, Schrottmaier WC, Salzmann M, et al. Platelet interaction with innate immune cells. *Transfus Med Hemother* 2016; 43: 78–88.
44. Kapur R and Semple JW. The nonhemostatic immune functions of platelets. *Semin Hematol* 2016; 53: S2–S6.
45. Zuchtriegel G, Uhl B, Puhr-Westerheide D, et al. Platelets guide leukocytes to their sites of extravasation. *PLoS Biol* 2016; 14: e1002459.
46. Seaman SA, Cao Y, Campbell CA, et al. Macrophage recruitment and polarization during collateral vessel remodeling in murine adipose tissue. *Microcirculation* 2016; 23: 75–87.
47. Gong L, Zhao Y, Zhang Y, et al. The macrophage polarization regulates MSC osteoblast differentiation in vitro. *Ann Clin Lab Sci* 2016; 46: 65–71.
48. Mountziaris PM, Spicer PP, Kasper FK, et al. Harnessing and modulating inflammation in strategies for bone regeneration. *Tissue Eng Part B Rev* 2011; 17: 393–402.
49. Loi F, Córdova LA, Pajarinen J, et al. Inflammation, fracture and bone repair. *Bone* 2016; 86: 119–130.
50. Debels H, Galea L, Han X-L, et al. Macrophages play a key role in angiogenesis and adipogenesis in a mouse tissue engineering model. *Tissue Eng Part A* 2013; 19: 2615–2625.
51. Buechler C, Krautbauer S and Eisinger K. Adipose tissue fibrosis. *World J Diabetes* 2015; 6: 548–553.
52. Li X, Li J, Wang L, et al. The role of metformin and resveratrol in the prevention of hypoxia-inducible factor 1α accumulation and fibrosis in hypoxic adipose tissue. *Br J Pharmacol* 2016; 173: 2001–2015.
53. Chen YC, Lin RZ, Qi H, et al. Functional human vascular network generated in photocrosslinkable gelatin methacrylate hydrogels. *Adv Funct Mater* 2012; 22: 2027–2039.